Spatial Correlation between Fluctuating and Static Fields over Metal and Dielectric Substrates

Martin Héritier,[1] Raphael Pachlatko,[1] Ye Tao,[2] John M. Abendroth,[1] Christian L. Degen,[1] and Alexander Eichler[1,*]
[1]Laboratory for Solid State Physics, ETH Zürich, CH-8093 Zürich, Switzerland
[2]Rowland Institute at Harvard, 100 Edwin H. Land Blvd., Cambridge, Massachusetts 02142, USA

(Received 9 April 2021; accepted 11 October 2021; published 15 November 2021)

We report spatially resolved measurements of static and fluctuating electric fields over conductive (Au) and nonconductive (SiO_2) surfaces. Using an ultrasensitive "nanoladder" cantilever probe to scan over these surfaces at distances of a few tens of nanometers, we record changes in the probe resonance frequency and damping that we associate with static and fluctuating fields, respectively. We find static and fluctuating fields to be spatially correlated. Furthermore, the fields are of similar magnitude for the two materials. We quantitatively describe the observed effects on the basis of trapped surface charges and dielectric fluctuations in an adsorbate layer. Our results are consistent with organic adsorbates significantly contributing to surface dissipation that affects nanomechanical sensors, trapped ions, superconducting resonators, and color centers in diamond.

DOI: 10.1103/PhysRevLett.127.216101

Introduction.—The last decades have seen rapid progress in the design and operation of devices for quantum applications. Today, we can build highly coherent qubits and resonators in optical, electrical, and mechanical media, and interface these platforms with each other to create hybrid systems [1–6]. Many important advances became possible through a reduction of the critical dimensions to the nanoscale, making the devices increasingly susceptible to the harmful influence of microscopic degrees of freedom that fluctuate in time. The coherence of trapped ions [7–11] and of superconducting Josephson circuits [12–14], for instance, is limited by fluctuating electrical fields. Evidence points to two-level systems in surface oxides and adsorbates as the microscopic origin of these fields [8,15–17]. Similar surface effects could also explain the poorly understood noncontact dissipation between closely spaced bodies that presents an obstacle for ultrasensitive scanning force microscopy [18–27]. Fluctuating electric fields furthermore affect the coherence of Rydberg atoms [28], color centers in diamond [29,30], and nanomechanical resonators [31,32].

In spite of the importance of understanding and overcoming these issues, the precise nature of the fluctuating fields is not sufficiently understood and remains the subject of an ongoing debate. This is largely due to experimental challenges. For instance, while atomic force microscopy (AFM) enables direct surface imaging, it usually lacks the sensitivity required to obtain conclusive evidence on noncontact dissipation beyond a few nanometers distance. Trapped ions, which are ideally suited for such investigations due to their high sensitivity, currently do not offer the imaging possibilities and nanoscale resolution of scanning probe methods [33]. For this reason, most previous studies relied on power laws of fluctuating forces or fields as a function of temperature, frequency, or distance [18,21,24–27,34–40]. Such studies, however, are difficult to interpret: on the one hand, a single model can produce different power laws at different distances [10] or temperatures [39,40]. On the other hand, various microscopic effects can combine to produce complex phenomena that thwart attempts at a simple explanation [16].

In this work, we report direct, experimental evidence for the connection between fluctuating electrical fields and static potential variations close to sample surfaces. To this end, we employ a "nanoladder" scanning force sensor that can detect force noise on the level of $1\mathrm{aN}/\sqrt{\mathrm{Hz}}$ [41]. This ultrasensitive probe allows us to produce scans of the noncontact dissipation a few tens of nm above surfaces. For comparison, we perform measurements over a metal (Au) and a dielectric (SiO_2). Over both substrates, we find that regions of high and low dissipation correlate with shifts of the mechanical resonance frequency that are attributed to "voltage patches" [42–47]. We can reproduce our observations using an established model [23] for electrical field fluctuation in dielectrics together with basic assumptions [11]. Our study provides a key to the understanding of surface dissipation effects and a potential route for improving the coherence of many types of quantum devices.

Device and setup.—Our scanning force probe is a pendulum-style nanoladder cantilever made of single-crystal Si, see Fig. 1(a) [41]. The cantilever has a bare resonance frequency of $f_0 = 4.858$ kHz, an effective mass of $m = 2.6$ pg, and a quality factor of $Q_0 = 26\,100$, corresponding to a spring constant $k_0 = m4\pi^2 f_0^2 = 2.4\ \mu\mathrm{N\,m^{-1}}$ and a damping coefficient $\Gamma_0 = m2\pi f_0/Q_0 = 3.1 \times 10^{-15}\ \mathrm{kg\,s^{-1}}$. To obtain a sharp, clean scanning tip,

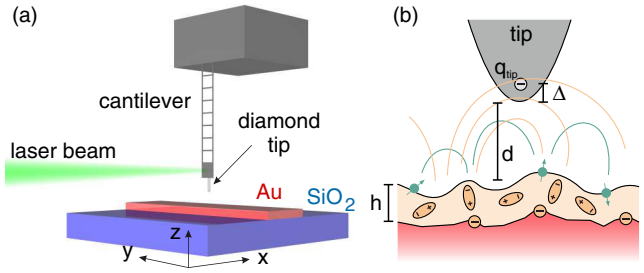

FIG. 1. Experimental setup. (a) A nanoladder cantilever oscillates parallel to the surface in the x direction. It is scanned over a sample surface consisting of SiO_2 and a pattern of Au that is 250 nm thick and electrically grounded. (b) Schematic representation of the diamond tip interacting with electrical (magnetic) fields generated by charge (spin) defects close to the sample surface. A bright orange area indicates an adsorbant layer, and q_{tip} represents a tip charge with a distance Δ to the tip apex.

we attach a diamond nanowire [48,49] to the end of the cantilever with a micromanipulator. The displacement of the cantilever is detected by fiber-optical interferometry with a 1550 nm laser [41,50]. Measurements are conducted in ultrahigh vacuum at a temperature of about 4 K.

Experimental results.—Our sample surface is a Si substrate with 1500 nm of thermally grown SiO_2. A region of the surface is covered with a 250 nm-thick Au film by e-beam evaporation; see Fig. 1. We begin our investigations by recording maps of the cantilever frequency f at constant tip height, corresponding to the mean tip-surface distance d; see Figs. 2(a)–2(b). The maps reveal distinct, reproducible variations in f on a length scale of 50–150 nm. Next, we perform linescans at different values of d and extract f and the quality factor Q from repeated ring-down measurements at every scan position, see Figs. 2(c)–2(d). Data acquisition per point takes 100–300 s for this procedure. From these measurements, we can determine the coefficient of noncontact friction Γ_{NCF} as

$$\Gamma_{\mathrm{NCF}} = \Gamma - \Gamma_0 = \frac{2\pi f m}{Q} - \frac{2\pi f_0 m}{Q_0}. \tag{1}$$

We observe significant variations of Γ_{NCF} at constant d over both materials, see Figs. 2(e)–2(f). Further, the variations in Γ_{NCF} correlate with those of f; maxima of f correspond to minima of Γ_{NCF} and vice versa. The variations smoothen out when increasing d. For $d \geq 100$ nm, we retrieve the intrinsic damping of the cantilever, $\Gamma \approx \Gamma_0$.

Figure 3 summarizes the quantitative analysis of our data. First, we observe a general increase of the variations in both f and Γ_{NCF} with decreasing d over both materials. Second, a strong increase of the mean value of Γ_{NCF} with decreasing d is detected. Third, a correlation between f and Γ_{NCF} is apparent close to the surface. These features are reproducible over surfaces of Au as well as SiO_2 at different

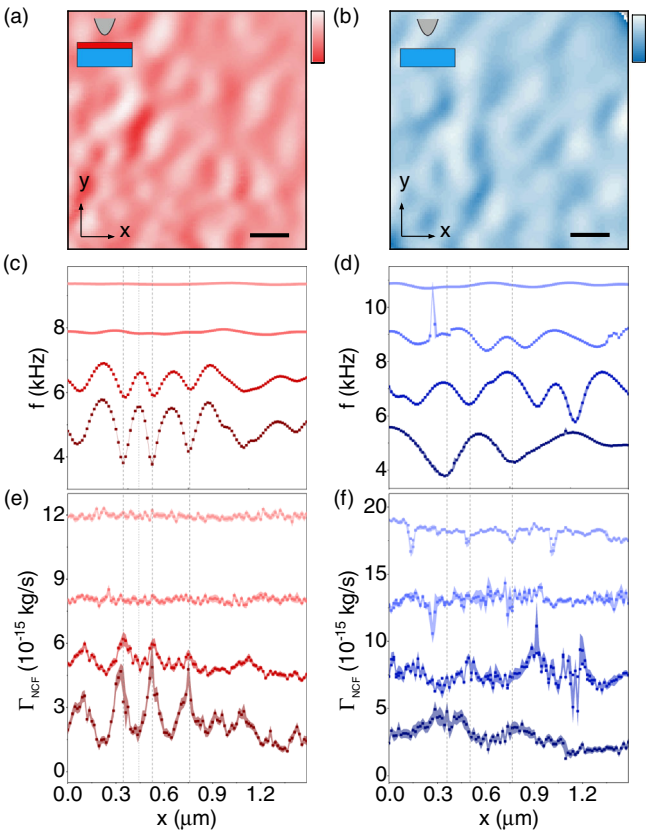

FIG. 2. Scanning results. (a) Maps of the cantilever frequency f recorded at a distance $d = 30$ nm over Au and (b) $d = 80$ nm over SiO_2. The colors range from red (4500) to white (5000 Hz) in (a) and from blue (4200) to white (5210 Hz) in (b). Both scale bars are 100 nm long. Insets show the tip over the substrate, SiO_2 (blue) and Au (red). (c)–(f) Line scans of the resonance frequency f and noncontact friction Γ_{NCF} over Au (c),(e) and SiO_2 (d),(f). The lines corresponds to $d = 30$, 45, 100, and 150 nm for Au and $d = 45$, 60, 75, and 100 nm for SiO_2 (bottom to top). Lines are offset for better visibility by 1.5 kHz each in (c), 2 kHz each in (d), 4×10^{-15} kg s^{-1} each in (e) and 6×10^{-15} kg s^{-1} each in (f). Shaded areas denote errors estimated from repeated measurements. Lateral drift may have occurred between the different line scans in (d) and (f). With our compact nanopositioners, drift can be caused by piezo creep after z approaches performed to ensure correct d calibration between the line scans.

positions over the sample, after thermal cycling to room temperature, and with magnetic fields up to 4 T (cf. Supplemental Material [51]). The results clearly point to nonuniform electric fields generated in a surface layer that must be present without regard of the substrate material underneath. In the following, we discuss concrete models that can explain our measurements.

Model.—When brought close to a material, the probe tip interacts with electrical or magnetic surface fields; cf. Fig. 1(b). In general, static fields are expected to modify the cantilever's potential energy E_{pot}, and therefore the spring constant $k = \delta^2 E_{\mathrm{pot}}/\delta x^2$ and the resonance

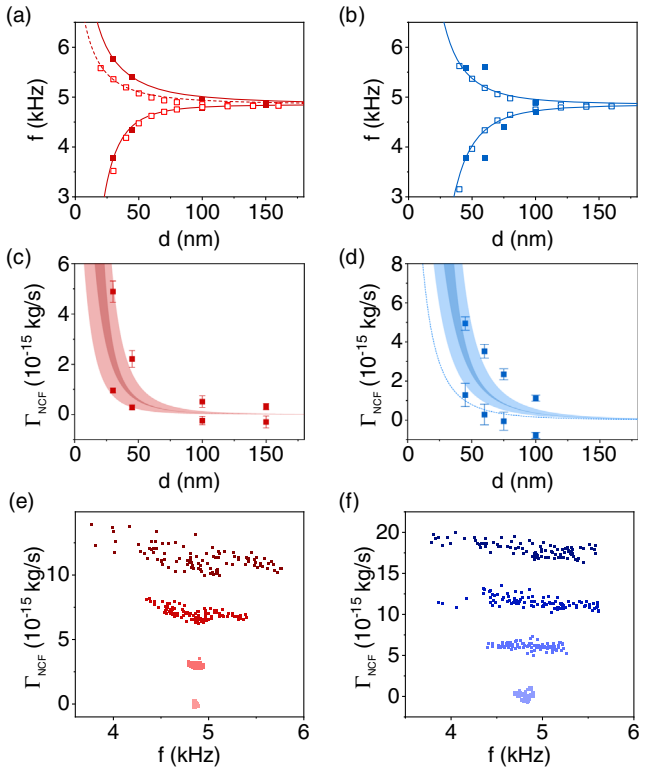

FIG. 3. Quantitative data analysis. (a) Maximum and minimum f as a function of d over Au and (b) over SiO_2. Filled and open squares correspond to our measurements and to model calculations, respectively. Solid lines are phenomenological fits using $f_0 \pm \beta_\pm/(d+\Delta)^{\nu_\pm}$. For Au, $\beta_- = 3\times10^{-23}$ Hz m$^{3.5}$ and $\nu_- = 3.5$, $\beta_+ = 2.3\times10^{-12}$ Hz m^2 and $\nu_+ = 2$ ($\beta_+ = 1.25\times10^{-12}$ Hz m^2 for the dashed line). For SiO_2, $\beta_- = 7.5\times10^{-23}$ Hz m$^{3.5}$ and $\nu_- = 3.5$, $\beta_+ = 1.8\times10^{-19}$ Hz m^3 and $\nu_+ = 3$. See main text and Supplemental Material for details on the model [51]. (c) Measured Γ_{NCF} and corresponding model for Au and (d) for SiO_2. Squares indicate the maxima and minima of a linescan at a distance d. The shaded areas corresponds to the model predictions for varying f [cf. solid lines in (a)–(b)] for $h = 1.0$ nm (dark shade) and for h between 0.4 and 2.0 nm (bright shade). We use $q_{tip} = q_e$ for both models, $\epsilon = 2$ and $\tan\theta = 0.01$ for Au, and $\epsilon = 2$ and $\tan\theta = 0.03$ for SiO_2. The dashed line in (d) is the additive dielectric contribution of the SiO_2 substrate with a thickness of 1.5 μm, $\epsilon = 4.44$ and $\tan\theta = 10^{-3}$. (e) Measured Γ_{NCF} as function of f for different d as in Fig. 2 over Au and (f) over SiO_2. Datasets are offset for better visibility by 3×10^{-15} kg s^{-1} each for Au and 5×10^{-15} kg s^{-1} each for SiO_2.

frequency $f = (1/2\pi)\sqrt{k/m}$ [55]. Local variation of the electrical surface potential, dubbed "voltage patches," were previously observed for various materials, and ascribed to trapped charges or work function differences for different crystalline facets [42–47,56]. Irrespective of their microscopic origin, we model such voltage patches as isolated charges q_i trapped at the surface. For a pointlike tip with a charge q_{tip}, shifts in f can be computed from the added electrostatic potential energy $E_{el} = \sum_i E_i$, where

$$E_i = \frac{1}{4\pi\epsilon_0}\frac{q_i q_{tip}}{r_i} \tag{2}$$

is the Coulomb energy of a surface charge q_i, with r_i the distance to the cantilever charge q_{tip}. With an electrostatic spring constant $k_{el} = \delta^2 E_{el}/\delta x^2$, we obtain

$$f = \frac{1}{2\pi}\sqrt{\frac{k_0}{m}+\frac{k_{el}}{m}} \approx f_0 + \frac{k_{el}}{8\pi^2 m f_0}, \tag{3}$$

where the last term is valid in the limit of $k_{el} \ll k_0$.

This simple electrostatic model can reproduce all main features of our frequency scans. The open dots in Fig. 3(a) show the maximum and minimum frequencies calculated for a square lattice of charges $q_i q_{tip} = 0.7 q_e^2$, where $q_e = 1.6\times10^{-19}$ C is the elementary charge and 0.7 is an arbitrary scaling factor chosen for best agreement with the experimental data. The model uses a site separation of 150 nm and an offset of $\Delta = 20$ nm between the tip apex and the position of the effective charge to emulate the shape of the line scans in Fig. 2(c). The offset roughly corresponds to the expected tip apex radius, cf. Supplemental Material for details [51]. For SiO_2, the same model with $q_i q_{tip} = 1.6 q_e^2$ yields best agreement with the experiment, see Fig. 3(b). The measured and simulated $f_{min,max}$ can be described by phenomenological power laws as described in the figure caption. The model is slightly asymmetric with respect to f_0 owing to the difference between the condition for negative f shifts (directly over a charge) and positive shifts (far from charges). This difference can be observed in the experiment as well, for instance, for $d = 30$ nm in Fig. 2(c). The asymmetry appears to be weaker in the experimental data than in the model, which may be due to a spatial spread of the effective charges in the tip.

While static field gradients give rise to frequency shifts, dissipation is identified as a signature of fluctuating fields. Previous studies have addressed the role of fluctuating electrical or magnetic defects at surfaces for dissipation, both in the contexts of scanning force microscopy [19–23,25–27] and, with a very similar framework, for trapped ions [7–11]. These results established that electrical fluctuations intrinsic to the substrate, such as thermally excited currents or tip-induced mirror charges in a conductor, produce negligible effects under most circumstances [11,18–20]. An alternative source of electrical fluctuations could be attributed to thin layers of adsorbants, such as hydrocarbons, that cover a surface immediately upon exposure to air [11,21,44,57]. As our cryogenic system does not permit baking out of the sample chamber, we must assume such adsorbant layers to be present. The most basic model for understanding Γ_{NCF}, therefore, is based on thermal dielectric fluctuations in a thin layer covering the sample surfaces. We verified with additional measurements that the dominant contribution to Γ_{NCF}

cannot be assigned to fluctuating surface electron spins, cf. Supplemental Material [25,51].

We use the model derived in Ref. [23] to determine the value of Γ_{NCF} expected for a thin dielectric. For the adsorbate layer on Au, we use as typical values a relative permittivity $\epsilon = 2$ and a loss tangent $\tan\theta = 0.01$ [11,58]. Defining the complex permittivity ϵ_c as

$$\epsilon_c = \epsilon(1 + i\tan\theta), \tag{4}$$

as well as the functions

$$\zeta = \frac{\epsilon_c - 1}{\epsilon_c + 1}, \tag{5}$$

$$J_2 = \int_0^\infty \frac{(1 - \mathrm{e}^{-4u(h/d)})u^2\mathrm{e}^{-2u}du}{(1 + \zeta'\mathrm{e}^{-2u(h/d)})^2 + (\zeta''\mathrm{e}^{-2u(h/d)})^2}, \tag{6}$$

where $'$ and $''$ denote the real and imaginary parts, respectively, the dissipation is calculated as [23]

$$\Gamma_{\mathrm{NCF}} = \frac{q_{\mathrm{tip}}^2\zeta''}{8\pi^2\epsilon_0 f d^3} J_2, \tag{7}$$

with ϵ_0 being the permittivity of free space, and h the adsorbed layer thickness. Note that Eq. (7) describes the situation of a dielectric on a metal substrate, but we use it also to approximate the adsorbate layer on SiO_2. In the Supplemental Material, we present a comparison to a second model that depicts the situation of two nonconducting layers and leads to very similar results [51,59].

Neither the effective tip charge q_{tip} nor its exact position in the diamond lattice is controlled in our experiment. The offset of $\Delta = 20$ nm between the tip apex and the charge position that we introduced for the electrostatic model is included for the dissipation calculations as well. From a rough experimental calibration of the effective tip charge, we get an upper bound of about $20q_e$ (cf. Supplemental Material [51]). However, the relevant number of charges must be significantly lower, because the calibration is sensitive to charges on distances of several μm, while our experiments only probe interactions on a scale of $d < 100$ nm, cf. Figs. 3(a)–3(d). We obtain best results assuming $q_{\mathrm{tip}} \approx q_e$.

There are several ways how Eq. (7) can be used to explain the experimentally observed variation in Γ_{NCF}. We start by noting that Eq. (7) has an explicit dependency $\Gamma_{\mathrm{NCF}} \propto f^{-1}$, producing the correct trend seen in Fig. 2. However, the variation of Γ_{NCF} generated in this way is too small to explain our experimental results, see dark shaded area in Figs. 3(c)–3(d), suggesting that additional effects are taking place in parallel. For instance, it was previously found that the thickness of hydrocarbon layers on Au is typically between $h = 0.4$ (a monolayer) and 2.0 nm [11,60,61]. Inserting such a variation in h into Eq. (7) yields a surprisingly close agreement with our measurements for Au, see Fig. 3(c). For SiO_2, the layer thickness required to reproduce our measurement for the given dielectric parameters is about 8 nm, which appears unrealistic. Instead, we present in Fig. 3(d) a model calculation with the same thickness variation as in (c), but with $\tan\theta = 0.03$. X-ray photoelectron spectroscopy measurements suggest that the chemical composition and bonding nature of the adventitious carbon on the two surfaces is indeed not identical (cf. Supplemental Material [51]). Considering the open questions regarding dielectric properties of nanometer-scale surface layers, the agreement that we find for both datasets is encouraging. Finally, we also obtain reasonable results when considering variations in d. For a thin dielectric layer ($h \ll d$), Eq. (7) yields approximately $\Gamma_{\mathrm{NCF}} \propto d^{-4}$, resulting in dissipation variations due to sample topography. The surfaces investigated in this work, Au and SiO_2, show different surface roughness and grain size in AFM topographic scans (see Supplemental Material [51]). This difference make an interpretation of the f variations in Figs. 2(a)–2(b) in terms of topographic features improbable. Finally, the expected Ohmic loss for bare Au [11] turns out to be about 10 orders of magnitude smaller than the measured values of Γ_{NCF}, ruling out a contribution due to mirror charges in a conductor. In conclusion, it is likely that dielectric fluctuations in a thin surface layer are the dominant cause of noncontact friction in our system.

Discussion.—We have set out to investigate the surface dissipation over different materials, selecting Au as a representative metal and SiO_2 as a dielectric. Our measurements provide evidence for a correlation between f and Γ_{NCF} over both substrates despite their different electronic properties. The plots in Figs. 3(e)–3(f) suggest $\Gamma_{\mathrm{NCF}} \propto f^{-1}$, even though the explicit f^{-1} dependency in Eq. (7), in concert with the measured variations in f, is not sufficient to explain the experimentally observed variations in Γ_{NCF}. We propose a simple model where minima (maxima) of f coincide either with maxima (minima) of h or with minima (maxima) of d. The microscopic mechanisms behind such correlations are at present speculative, but appear to originate from the electrostatic voltage patches close to the surface. For instance, surface potential patches exert attractive forces onto molecules with a dipole moment, which can lead to site-selective adsorption [44] and a maximum of h directly over static charges. Alternatively, a correlation between topographic features (d) and static charges is to be expected if the voltage patches are generated by differences in the surface work function at crystallographic grain orientations, as proposed in Ref. [46].

With a tip charge estimated as $q_{\mathrm{tip}} = q_e$, we can quantify the power spectral density of the fluctuating electrical field as

$$S_E = 4k_B T \Gamma_{\mathrm{NCF}}/q_e^2. \quad (8)$$

The values we obtain from Eq. (8) are in the range of $10-100\ \mathrm{V^2\,m^{-2}\,Hz^{-1}}$, which is 10^{11}–10^{15} times larger than what is typically detected with trapped ions [10]. This discrepancy is not surprising, because the distance to the surface d in our measurements is about 10^3–10^4 times smaller than in an ion-trap experiment. With the phenomenological power law $\Gamma_{\mathrm{NCF}} \propto d^{-4}$ that we obtained in the thin-film limit from Eq. (7), we should expect a difference by a factor 10^{12}–10^{16}.

It is worth comparing our work to previous studies of fluctuating electrical fields with nanomechanical sensors in the $d = 10-100$ nm range [18,21,34]. We note that those studies concentrated mostly on the d^{-n} dependence at single points over a sample. The values of n that were found varied strongly, from $1 < n < 1.5$ in Ref. [18] to $n \geq 3$ in Ref. [34]. Our experimental data are in rough agreement with the exponent $n \approx 4$ predicted for thin dielectric layers [21,23].

Conclusion and outlook.—We identify surface adsorbants as the likely origin of noncontact friction over conducting and insulating materials. This result resolves much of the previous disagreement between experiments and models—even over superconducting surfaces, such thin dielectric layers are often unavoidable. (A notable exception is the experiment from Kisiel *et al.* [24] that was conducted after baking out the vacuum chamber.) A second finding is that the fluctuating electrical fields vary spatially and are correlated with static surface potentials. This provides an important clue to the formation of adsorbants and, potentially, a strategy to reduce their impact through chemical functionalization with molecular monolayers that feature tailored electronic properties [62]. Such a strategy would benefit many of the most advanced fields in quantum sensing and quantum computation, in particular trapped ions, superconducting qubits and ultrasensitive force probes [4,10,11,14,63]. In a next step, the microscopic nature of surface layers can be investigated with magnetic resonance force microscopy [63–65] or other scanning tools like nanoscale SQUIDS [66,67] or diamond probes with optically active nitrogen-vacancy defects [68–70].

We gratefully acknowledge discussions with Jonathan Home, Thomas Ihn, Marc-Dominik Krass, Roger Loring, John Marohn, Clemens Müller, and Oded Zilberberg, the MRFM team of the Degen group, as well as technical support by U. Grob and P. Märki. This work is supported by the Swiss National Science Foundation (SNSF) through the Sinergia Project ZEPTO, Grant No. CRSII5_177198/1, the National Center of Competence in Research in Quantum Science and Technology, an ETH Research Grant ETH-03 16-1, and the FIRST clean room facility at ETH. Ye Tao is supported by a Rowland Fellowship.

*eichlera@phys.ethz.ch

[1] L.-M. Duan and C. Monroe, Rev. Mod. Phys. **82**, 1209 (2010).
[2] Z.-L. Xiang, S. Ashhab, J. Q. You, and F. Nori, Rev. Mod. Phys. **85**, 623 (2013).
[3] M. Aspelmeyer, T. J. Kippenberg, and F. Marquardt, Rev. Mod. Phys. **86**, 1391 (2014).
[4] C. L. Degen, F. Reinhard, and P. Cappellaro, Rev. Mod. Phys. **89**, 035002 (2017).
[5] C. D. Bruzewicz, J. Chiaverini, R. McConnell, and J. M. Sage, Appl. Phys. Rev. **6**, 021314 (2019).
[6] M. Kjaergaard, M. E. Schwartz, J. Braumüller, P. Krantz, J. I.-J. Wang, and S. Gustavsson, and W. D. Oliver, Annu. Rev. Condens. Matter Phys. **11**, 369 (2020).
[7] Q. A. Turchette, D. Kielpinski, B. E. King, D. Leibfried, D. M. Meekhof, C. J. Myatt, M. A. Rowe, C. A. Sackett, C. S. Wood, W. M. Itano, C. Monroe, and D. J. Wineland, Phys. Rev. A **61**, 063418 (2000).
[8] J. Labaziewicz, Y. Ge, D. R. Leibrandt, S. X. Wang, R. Shewmon, and I. L. Chuang, Phys. Rev. Lett. **101**, 180602 (2008).
[9] A. Safavi-Naini, P. Rabl, P. F. Weck, and H. R. Sadeghpour, Phys. Rev. A **84**, 023412 (2011).
[10] M. Brownnutt, M. Kumph, P. Rabl, and R. Blatt, Rev. Mod. Phys. **87**, 1419 (2015).
[11] M. Kumph, C. Henkel, P. Rabl, M. Brownnutt, and R. Blatt, New J. Phys. **18**, 023020 (2016).
[12] J. Gao, M. Daal, A. Vayonakis, S. Kumar, J. Zmuidzinas, B. Sadoulet, B. A. Mazin, P. K. Day, and H. G. Leduc, Appl. Phys. Lett. **92**, 152505 (2008).
[13] H. Wang, M. Hofheinz, J. Wenner, M. Ansmann, R. C. Bialczak, M. Lenander, E. Lucero, M. Neeley, A. D. OConnell, D. Sank, M. Weides, A. N. Cleland, and J. M. Martinis, Appl. Phys. Lett. **95**, 233508 (2009).
[14] C. Mller, J. H. Cole, and J. Lisenfeld, Rep. Prog. Phys. **82**, 124501 (2019).
[15] D. Allcock, L. Guidoni, T. Harty, C. Ballance, M. Blain, A. Steane, and D. Lucas, New J. Phys. **13**, 123023 (2011).
[16] D. A. Hite, Y. Colombe, A. C. Wilson, K. R. Brown, U. Warring, R. Jordens, J. D. Jost, K. S. McKay, D. P. Pappas, D. Leibfried, and D. J. Wineland, Phys. Rev. Lett. **109**, 103001 (2012).
[17] A. Safavi-Naini, E. Kim, P. F. Weck, P. Rabl, and H. R. Sadeghpour, Phys. Rev. A **87**, 023421 (2013).
[18] B. C. Stipe, H. J. Mamin, T. D. Stowe, T. W. Kenny, and D. Rugar, Phys. Rev. Lett. **87**, 096801 (2001).
[19] A. I. Volokitin and B. N. J. Persson, Phys. Rev. B **68**, 155420 (2003).
[20] J. R. Zurita-Sanchez, J.-J. Greffet, and L. Novotny, Phys. Rev. A **69**, 022902 (2004).
[21] S. Kuehn, R. F. Loring, and J. A. Marohn, Phys. Rev. Lett. **96**, 156103 (2006).
[22] A. I. Volokitin and B. N. J. Persson, Rev. Mod. Phys. **79**, 1291 (2007).
[23] S. M. Yazdanian, J. A. Marohn, and R. F. Loring, J. Chem. Phys. **128**, 224706 (2008).
[24] M. Kisiel, E. Gnecco, U. Gysin, L. Marot, S. Rast, and E. Meyer, Nat. Mater. **10**, 119 (2011).
[25] J.-H. She and A. V. Balatsky, Phys. Rev. Lett. **108**, 136101 (2012).

[26] A. M. J. denHaan, J. J. T. Wagenaar, J. M. de Voogd, G. Koning, and T. H. Oosterkamp, Phys. Rev. B **92**, 235441 (2015).
[27] J. M. de Voogd, J. J. T. Wagenaar, and T. H. Oosterkamp, Sci. Rep. **7**, 42239 (2017).
[28] J. D. Carter and J. D. D. Martin, Phys. Rev. A **88**, 043429 (2013).
[29] M. Kim, H. J. Mamin, M. H. Sherwood, K. Ohno, D. D. Awschalom, and D. Rugar, Phys. Rev. Lett. **115**, 087602 (2015).
[30] P. Jamonneau, M. Lesik, J. P. Tetienne, I. Alvizu, L. Mayer, A. Dréau, S. Kosen, J.-F. Roch, S. Pezzagna, J. Meijer, T. Teraji, Y. Kubo, P. Bertet, J. R. Maze, and V. Jacques, Phys. Rev. B **93**, 024305 (2016).
[31] Y. Tao, P. Navaretti, R. Hauert, U. Grob, M. Poggio, and C. L. Degen, Nanotechnology **26**, 465501 (2015).
[32] M. Hamoumi, P. E. Allain, W. Hease, E. Gil-Santos, L. Morgenroth, B. Gérard, A. Lemaître, G. Leo, and I. Favero, Phys. Rev. Lett. **120**, 223601 (2018).
[33] R. Maiwald, D. Leibfried, J. Britton, J. C. Bergquist, G. Leuchs, and D. J. Wineland, Nat. Phys. **5**, 551 (2009).
[34] B. Gotsmann and H. Fuchs, Phys. Rev. Lett. **86**, 2597 (2001).
[35] S. M. Yazdanian, N. Hoepker, S. Kuehn, R. F. Loring, and J. A. Marohn, Nano Lett. **9**, 2273 (2009).
[36] K. Saitoh, K. Hayashi, Y. Shibayama, and K. Shirahama, Phys. Rev. Lett. **105**, 236103 (2010).
[37] J. Chiaverini and J. M. Sage, Phys. Rev. A **89**, 012318 (2014).
[38] C. D. Bruzewicz, J. M. Sage, and J. Chiaverini, Phys. Rev. A **91**, 041402(R) (2015).
[39] J. A. Sedlacek, J. Stuart, D. H. Slichter, C. D. Bruzewicz, R. McConnell, J. M. Sage, and J. Chiaverini, Phys. Rev. A **98**, 063430 (2018).
[40] C. Noel, M. Berlin-Udi, C. Matthiesen, J. Yu, Y. Zhou, V. Lordi, and H. Haffner, Phys. Rev. A **99**, 063427 (2019).
[41] M. Héritier, A. Eichler, Y. Pan, U. Grob, I. Shorubalko, M. D. Krass, Y. Tao, and C. L. Degen, Nano Lett. **18**, 1814 (2018).
[42] J. B. Camp, T. W. Darling, and R. E. Brown, J. Appl. Phys. **69**, 7126 (1991).
[43] N. A. Burnham, R. J. Colton, and H. M. Pollock, Phys. Rev. Lett. **69**, 144 (1992).
[44] F. Rossi and G. I. Opat, J. Phys. D **25**, 1349 (1992).
[45] C. C. Speake and C. Trenkel, Phys. Rev. Lett. **90**, 160403 (2003).
[46] N. Gaillard, M. Gros-Jean, D. Mariolle, F. Bertin, and A. Bsiesy, Appl. Phys. Lett. **89**, 154101 (2006).
[47] N. A. Robertson, J. R. Blackwood, S. Buchman, R. L. Byer, J. Camp, D. Gill, J. Hanson, S. Williams, and P. Zhou, Classical Quantum Gravity **23**, 2665 (2006).
[48] Y. Tao and C. L. Degen, Nano Lett. **15**, 7893 (2015).
[49] Y. Tao, A. Eichler, T. Holzherr, and C. L. Degen, Nat. Commun. **7**, 12714 (2016).
[50] D. Rugar, H. Mamin, and P. Guethner, Appl. Phys. Lett. **55**, 2588 (1989).
[51] See Supplemental Material at http://link.aps.org/supplemental/10.1103/PhysRevLett.127.216101 for setup calibration, additional measurements, and details regarding the models, which includes Refs. [52–54].
[52] A. D. Sen, V. G. Anicich, and T. Arakelian, J. Phys. D **25**, 516 (1992).
[53] S. Sangtawesin, B. L. Dwyer, S. Srinivasan, J. J. Allred, L. V. H. Rodgers, K. De Greve, A. Stacey, N. Dontschuk, K. M. O'Donnell, D. Hu, D. A. Evans, C. Jaye, D. A. Fischer, M. L. Markham, D. J. Twitchen, H. Park, M. D. Lukin, and N. P. de Leon, Phys. Rev. X **9**, 031052 (2019).
[54] D. Martinez-Martin, R. Longuinhos, J. G. Izquierdo, A. Marele, S. S. Alexandre, M. Jaafar, J. M. Gómez-Rodríguez, L. Bañares, J. M. Soler, and J. Gomez-Herrero, Carbon **61**, 33 (2013).
[55] I. Kozinsky, H. C. Postma, I. Bargatin, and M. Roukes, Appl. Phys. Lett. **88**, 253101 (2006).
[56] J. Zúñiga-Pérez, V. Muñoz-Sanjosé, E. Palacios-Lidón, and J. Colchero, Phys. Rev. Lett. **95**, 226105 (2005).
[57] T. Smith, J. Colloid Interface Sci. **75**, 51 (1980).
[58] G. W. C. Kaye and T. H. Laby, *Tables of Physical and Chemical Constants* (Longman, Harlow, England, UK, 1995).
[59] S. Lekkala, J. A. Marohn, and R. F. Loring, J. Chem. Phys. **139**, 184702 (2013).
[60] C. Degen, M. Poggio, H. Mamin, C. Rettner, and D. Rugar, Proc. Natl. Acad. Sci. U.S.A. **106**, 1313 (2009).
[61] M. Loretz, S. Pezzagna, J. Meijer, and C. Degen, Appl. Phys. Lett. **104**, 033102 (2014).
[62] J. Thomas, J. Schwartz, J. Hohman, S. Claridge, H. Auluck, A. Serino, A. Spokoyny, G. Tran, K. Kelly, C. Mirkin, J. Gilles, S. Osher, and P. Weiss, ACS Nano **9**, 4734 (2015).
[63] M. Poggio and C. L. Degen, Nanotechnology **21**, 342001 (2010).
[64] W. Rose, H. Haas, A. Q. Chen, N. Jeon, L. J. Lauhon, D. G. Cory, and R. Budakian, Phys. Rev. X **8**, 011030 (2018).
[65] U. Grob, M. D. Krass, and M. Héritier, R. Pachlatko, J. Rhensius, J. Košata, B. A. Moores, H. Takahashi, A. Eichler, and C. L. Degen, Nano Lett. **19**, 7935 (2019).
[66] A. Finkler, Y. Segev, Y. Myasoedov, M. L. Rappaport, L. Neeman, D. Vasyukov, E. Zeldov, M. E. Huber, J. Martin, and A. Yacoby, Nano Lett. **10**, 1046 (2010).
[67] D. Vasyukov, L. Ceccarelli, M. Wyss, B. Gross, A. Schwarb, A. Mehlin, N. Rossi, G. Tütüncuöglu, F. Heimbach, R. Zamani, A. Kovács, A. Fontcuberta i Morral, D. Grundler, and M. Poggio, Nano Lett. **18**, 964 (2018).
[68] C. Degen, Appl. Phys. Lett. **92**, 243111 (2008).
[69] J. Maze, P. Stanwix, J. Hodges, S. Hong, J. Taylor, P. Cappellaro, L. Jiang, M. G. Dutt, E. Togan, A. Zibrov, A. Yacoby, R. L. Walsworth, and M. D. Lukin, Nature (London) **455**, 644 (2008).
[70] G. Balasubramanian, I. Chan, R. Kolesov, M. Al-Hmoud, J. Tisler, C. Shin, C. Kim, A. Wojcik, P. R. Hemmer, A. Krueger, T. Hanke, A. Leitenstorfer, R. Bratschitsch, F. Jelezko, and J. Wrachtrup, Nature (London) **455**, 648 (2008).